Eur Respir J, 1995, 8, 1001–1017
DOI: 10.1183/09031936.95.08061001
Printed in UK - all rights reserved

European Respiratory Journal
ISSN 0903 - 1936

REVIEW

Pulmonary studies using positron emission tomography

C.G. Rhodes*, J.M.B. Hughes**

Pulmonary studies using positron emission tomography. C.G. Rhodes, J.M.B. Hughes. ©ERS Journals 1995.

ABSTRACT: The detailed investigation of regional differences in lung function at a local level began when suitable γ-ray emitting isotopes and focused external radiation detectors (especially the Anger γ-camera) became available. A major recent advance has been the development of positron emission tomography (PET), which provides a powerful combination of highly accurate tomographic reconstruction of radioisotope concentration with a potentially unlimited list of biological compounds to be labelled with the positron emitting isotopes of oxygen, carbon and fluorine.

Early studies using PET focused on the inhalation of ^{11}CO (or $C^{15}O$) and ^{19}Ne gases and the intravenous injection of ^{13}N in saline and $H_2{}^{15}O$ for the measurement of relatively simple aspects of regional lung function, such as tissue, blood and gas volumes, blood flow, ventilation and ventilation/perfusion (V'_A/Q'). More recent work has been directed towards the more challenging areas of regional endothelial permeability, carbohydrate utilization, enzyme and receptor binding assays, and *in vivo* pharmacokinetics.

The short physical half-lives of the isotopes (17 s to 2 h) and the noninvasive nature of PET allows serial measurements to be made on patients (within the constraints of permitted radiation doses) to assess the effect of physiological and therapeutic interventions.

Eur Respir J., 1995, 8, 1001–1017.

*MRC Cyclotron Unit, Clinical Sciences Centre, Hammersmith Hospital, London, UK. **Dept of Medicine, Royal Postgraduate Medical School, Hammersmith Hospital, London, UK.

Correspondence: J.M.B. Hughes
Dept of Medicine
Royal Postgraduate Medical School
Hammersmith Hospital
London W12 0NN
UK

Keywords: *In vivo* autoradiography
positron emission tomography
regional lung function

Received: October 10 1994
Accepted after revision February 6 1995

Positron emission tomography (PET) is a specialized branch of medical imaging, whose accuracy and specificity merit the term "*in vivo* autoradiography". PET scans present their radioisotopic data in a three-dimensional format, in a series of transaxial sections through the thorax, just like an X-ray computed tomography (CT) scan. In contrast to the CT scan, however, these data maps contain physiological, biochemical and pharmacological information superimposed on the anatomical topography. Unlike traditional invasive methods, PET can "biopsy" the lung as often as the accumulated radiation dose permits. Lung PET scanning has been reviewed previously, in 1985 [1, 2] and 1989 [3].

Positron emitters differ from single photon emitting radionuclides, such as technetium-99m, in the following ways: 1) through electron annihilation, positrons emit two γ-rays of identical energy (511 keV) at 180° to each other; 2) the paired γ-rays are detected by coincidence counting, which eliminates the need for detector collimation, and permits accurate corrections of γ-ray attenuation; 3) positron emitters, in general, have short (2–110 min) physical half-lives; and 4) fundamental organic molecules (oxygen, nitrogen, carbon and fluorine (a surrogate for hydrogen)) are represented by positron emitters.

These attributes are very important. For example, with coincidence counting (see below) heavy shielding of the detectors for the 511 keV γ-rays is not required, and the attenuation corrections are sufficiently accurate for local concentrations of radioisotopes to be measured very precisely, with a well-defined geometry. The monoenergetic 511 keV γ-ray energy (common to all positron annihilation) means that different emitters, *e.g.* oxygen-15, carbon-11, fluorine-18, *etc.*, can be directly compared. The short physical half-lives allow serial measurements to be made with minimal background subtraction. The availability of carbon-11 and fluorine-18 for radiochemical synthesis gives positron emitters a distinct chemical advantage over the single photon emitters, where surrogates, such as technetium-99m and iodine-123, have to be used.

PET, of course, has some disadvantages, mainly technical and economic: *e.g.*, proximity to a cyclotron; specialized radiochemistry; relatively poor spatial resolution compared to CT and nuclear magnetic resonance (spectroscopy) (NMR) (*c.* 7 mm - full width at half maximum); scanning distance (cranial to caudal) currently limited to 15 cm (new machines are now being extended to cover 24 cm); and high capital and running costs.

The first two of these factors stem from the short half-lives of ^{15}O and ^{11}C. Spatial resolution is limited for pulmonary applications by the high positron energy and the low density of the lungs. Single photon emission computed tomography (SPECT) is a cheaper alternative to PET, but it lacks the selectivity, specificity and accuracy of PET. Consequently, PET is likely to remain the gold standard, and will always provide a far greater variety of biophysiological and pharmacokinetic information.

Positron detection

Properties of positrons

Radioactive isotopes have unstable atomic nuclei, which become stable by radioactive "decay". Positron emitters are unstable because of an excess positive charge, *i.e.* a deficiency of negatively charged electrons. Positrons and electrons have the same mass. Excess positrons escape from the nucleus and travel a short distance through tissues until they collide with a free electron. This distance is 2–10 mm, and depends on the number of electrons encountered (proportional to tissue density, which is variable in the case of the lung) and the kinetic energy of the positron. The result of the positron-electron interaction is "annihilation" - the emission of two 511 keV γ-rays travelling "back-to-back" at 180° to each other. All positron emitters, listed in table 1, emit the same 511 keV γ-energy.

Coincidence counting

If the two 511 keV γ-rays are detected simultaneously (within a 12 ns time window) by scintillation detectors facing each other (fig. 1a), there is a high probability that the source of the captured positron lies along a path connecting the two detectors. With a ring of detectors "in tomographic mode", the pattern of coincidences localizes the source even more precisely (fig. 1b). However, a number of these coincidences will be misplaced because of scatter of one or both of the γ-rays (fig. 1c). This depends on the geometry of the detector array and the object size, but cold spot phantoms show this to be of minor importance (<2% "spillover") when scanning "with septa" on whole body machines. In addition, a certain proportion of coincidences will occur between any two detectors simultaneously, simply by chance (fig. 1c). These "random" coincidences, which depend mainly on the number of single γ-rays recorded per second and the coincidence time interval, usually contribute less than 3% of total coincidences, and can be determined during scanning by simultaneously recording a second set of coincidences with a delayed time window (128 ns).

Attenuation correction

The chance of a coincidence occurring between detectors on opposite sides of the chest is diminished if there is dense tissue, such as the heart, in the path of one of either of the 511 γ-rays (fig. 1a). To take account of this, a correction procedure is adopted (fig. 1d). A ring source of a positron-emitting isotope (usually $^{68}Ge/^{68}Ga$) is placed in the detector field and scans are recorded: 1) with air (a blank); and 2) with the subject in position. The fraction of the original coincidences recorded by each detector pair represents the attenuation factor for that geometry. This is because the total attenuation path length (x to y in fig. 1b) is constant, no matter where the source is placed within a given detector pair field of view - which includes a point outside the body. PET scans obtained with the ring source exposed are called "transmission" scans, to distinguish them from "emission" scans when the radiation is coming from within the thorax.

The transmission scan provides a second very important piece of information, as pointed out by RHODES *et al*. [4]. In the tomographic mode, using coincidence detection, the attenuation factor for each projection is inversely proportional to the physical density of the intervening material. Therefore, after calibration, the reconstructed transmission scan (fig. 2a) provides a quantitative map of the tissue density distribution (D_L) (g (lung)·mL^{-1} thorax), rather like an X-ray computed tomography (CT) scan, but without the associated beam hardening problems.

Tomography

PET scanners look like CT scanners on the outside. Inside, they consist of adjacent rings of scintillation detectors (usually bismuth germanate) made up of blocks, often with slots cut to make eight sections, thus providing multiple planes of transaxial information [5]. For example, a "two-block 16-slice" machine will provide 31 planes of information from contiguous sections of thorax, each 3.5 mm wide, when "cross-plane" information between adjacent rings is utilized. This covers a distance of 10 cm - about 50% of the lung length at mid-tidal volume

Table 1. – Commonly used positron emitting radioisotopes and labelled compounds

Radionuclide	$T_{1/2}$	Chemical form	Use
^{11}C	20 min	^{11}C-CGP12177	Beta-receptor function
		^{11}C-5-hydroxytryptamine	Endothelial function
		^{11}C-chlorpromazine	Endothelial function
		^{11}C-erythromycin	Pharmacokinetics
		^{11}C-methyl albumin	Plasma volume-haematocrit ratio
^{13}N	10 min	$^{13}N_2$ in saline	V'/Q' ratios
^{15}O	2.1 min	$C^{15}O$	Red blood cell volume
		$C^{15}O_2$	Blood flow, lung water
		$H_2{}^{15}O$	Blood flow, lung water
^{18}F	110 min	^{18}F-deoxyglucose	Glucose metabolism
^{19}Ne	17.4 s	Gas	Ventilation
^{68}Ga	68 min	Transferrin bound	Vascular permeability

$T_{1/2}$: half-life; V'/Q': ventilation/perfusion ratio.

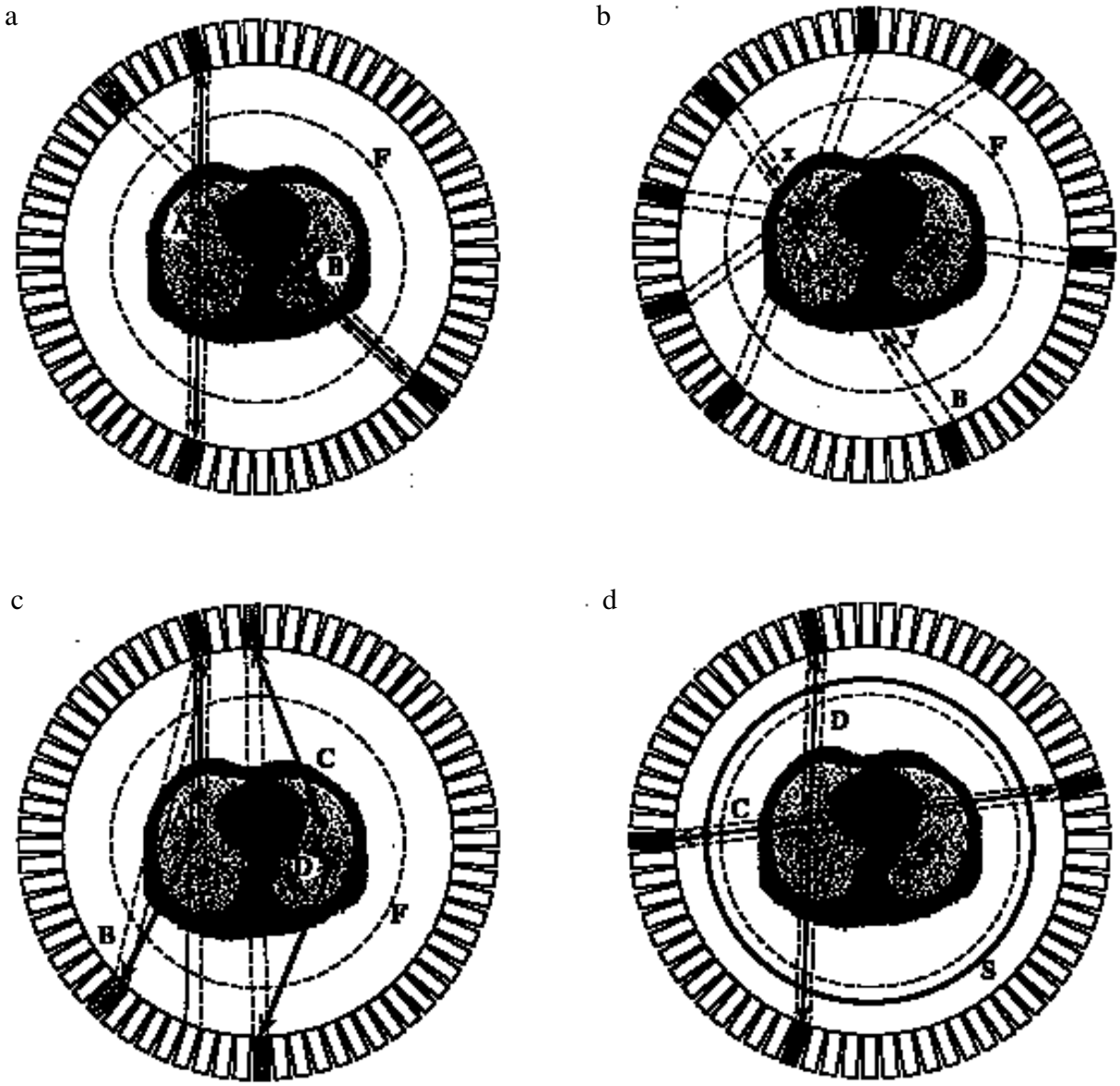

Fig. 1. – a) Diagrammatic representation of the positron emission tomography (PET) scanner showing the block design of the circular detector ring and a cross-sectional density map of the lower thorax at mid-heart level within the scanner field of view (F). Point A corresponds to the annihilation of a locally emitted positron, which is identified by the coincidence detection (within a 12 ns time window) of the resulting two γ-rays (bold arrows) emitted "back-to-back". The region viewed by this detector pair (black shaded areas) is indicated by the double broken line. The annihilation at point B illustrates how potential coincidences can be missed due to attenuation effects. One of the γ-rays is deflected out of the detector plane and is not recorded by the opposing detector (stippled area). b) Conceptually, the location of an isolated source of radioactivity within the body can be determined from the response of detector pairs viewing the region from different angles. The reconstruction algorithm converts the recorded distribution of true coincidences (the emission scan) into a tomographic distribution of isotope concentration (the emission image). Central to this is a correction for coincidence losses due to γ-ray attenuation by tissue. As can be seen from this figure, the total attenuating path length (*i.e.* for both γ-rays) for projection B is the distance x to y, irrespective of the position of the source within this region. c) Two common sources of error are illustrated: 1) Scatter - where a γ-ray resulting from an annihilation at A is deflected due to an interaction with tissue and detected by a neighbouring detector in the ring. The event is then recorded as an apparently true coincidence along the projection B. This misplacement of coincidences results in a small background in the reconstructed image of the order of 1–2%; 2) Randoms - where pairs of annihilations (at C and D, often occurring outside of the detector ring) each have a γ-ray recorded by a coincident detector pair (within the 12 ns time window). These coincident "singles" are then considered to arise from an original annihilation along the path shown. This error can be simply corrected for during the scan by simultaneously measuring the actual random count rate for a given coincident pair with the introduction of a long delay (128 ns) in the coincidence detection circuitry to exclude "true" coincidences. d) Attenuation measurements are made by recording a transmission scan after placing a ring source (bold line S) of a long-lived positron emitting isotope (usually $^{68}Ge/^{68}Ga$) between the subject and the detector ring. Fewer true coincidences are obtained for the detector pair recording γ-rays emitted from the annihilation at point C in the ring source than those from point D, because of the additional attenuating mass of the heart. The total attenuation path length for a given projection in the transmission scan is identical to that of the emission scan (*e.g.* x to y in fig. 1b). The transmission scan data are directly compared to a blank (transmission) scan, obtained by recording coincidences with the subject and bed out of the field of view, to obtain a quantitative measurement of the attenuation coefficients. This attenuation information is then applied to the emission scan prior to reconstruction of the final image. (Figure 1 has been redrawn from [3] with permission).

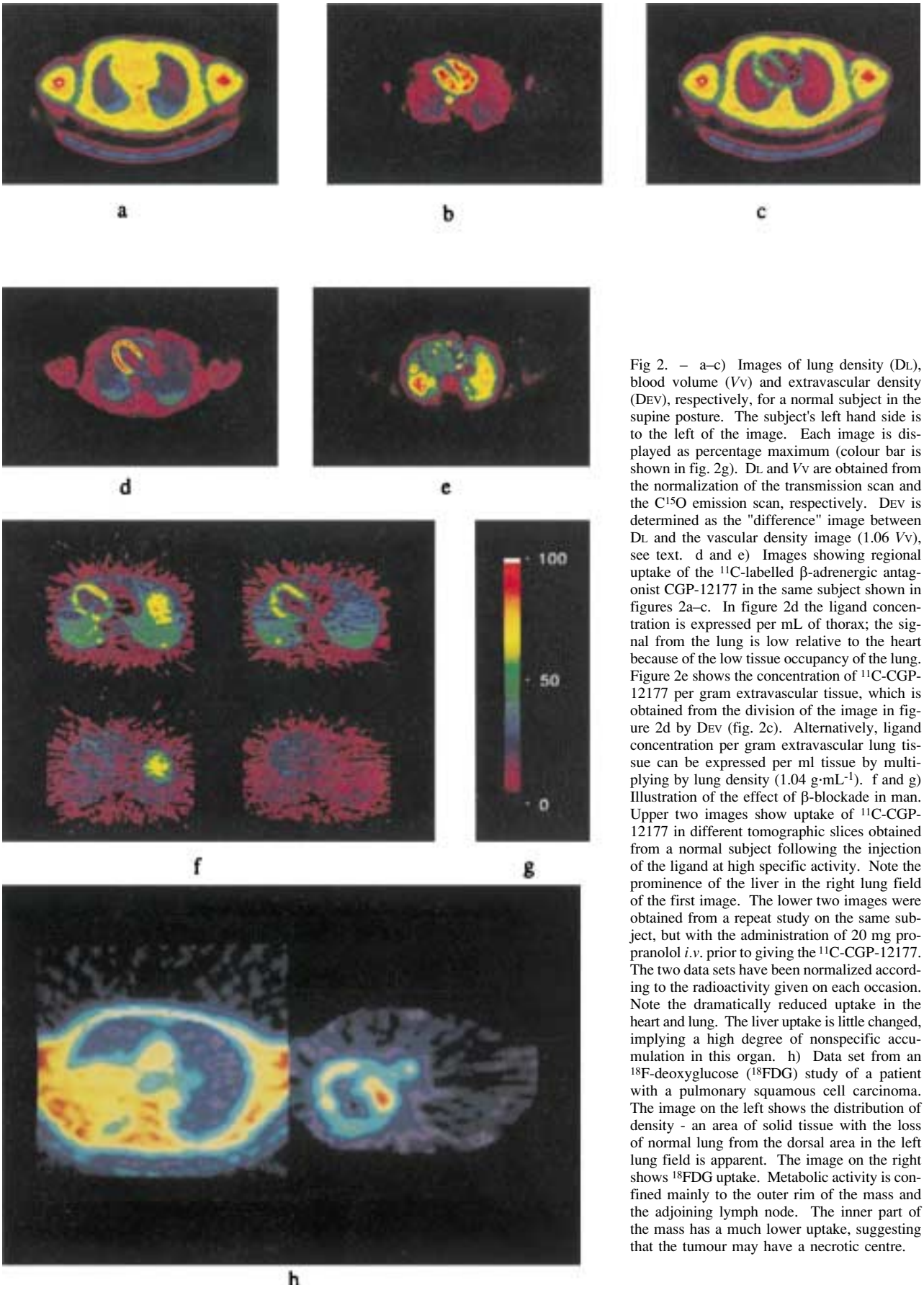

Fig 2. – a–c) Images of lung density (D_L), blood volume (V_V) and extravascular density (D_{EV}), respectively, for a normal subject in the supine posture. The subject's left hand side is to the left of the image. Each image is displayed as percentage maximum (colour bar is shown in fig. 2g). D_L and V_V are obtained from the normalization of the transmission scan and the $C^{15}O$ emission scan, respectively. D_{EV} is determined as the "difference" image between D_L and the vascular density image (1.06 V_V), see text. d and e) Images showing regional uptake of the ^{11}C-labelled β-adrenergic antagonist CGP-12177 in the same subject shown in figures 2a–c. In figure 2d the ligand concentration is expressed per mL of thorax; the signal from the lung is low relative to the heart because of the low tissue occupancy of the lung. Figure 2e shows the concentration of ^{11}C-CGP-12177 per gram extravascular tissue, which is obtained from the division of the image in figure 2d by D_{EV} (fig. 2c). Alternatively, ligand concentration per gram extravascular lung tissue can be expressed per ml tissue by multiplying by lung density (1.04 $g \cdot mL^{-1}$). f and g) Illustration of the effect of β-blockade in man. Upper two images show uptake of ^{11}C-CGP-12177 in different tomographic slices obtained from a normal subject following the injection of the ligand at high specific activity. Note the prominence of the liver in the right lung field of the first image. The lower two images were obtained from a repeat study on the same subject, but with the administration of 20 mg propranolol *i.v.* prior to giving the ^{11}C-CGP-12177. The two data sets have been normalized according to the radioactivity given on each occasion. Note the dramatically reduced uptake in the heart and lung. The liver uptake is little changed, implying a high degree of nonspecific accumulation in this organ. h) Data set from an ^{18}F-deoxyglucose (^{18}FDG) study of a patient with a pulmonary squamous cell carcinoma. The image on the left shows the distribution of density - an area of solid tissue with the loss of normal lung from the dorsal area in the left lung field is apparent. The image on the right shows ^{18}FDG uptake. Metabolic activity is confined mainly to the outer rim of the mass and the adjoining lymph node. The inner part of the mass has a much lower uptake, suggesting that the tumour may have a necrotic centre.

in a supine resting subject. If the most caudal section is placed at the apex of the right diaphragm, about 70% of the lung volume will be covered by the scan. It is only practical to make studies in the decubitus postures. The in-plane spatial resolution (full width half maximum (FWHM)) of current scanner is of the order of 8 mm in solid tissue. The resolution is worse in lung tissue because of the greater path length of the positrons in the less dense medium - say 15 mm, which approximately equals the diameter of two acini. The acinus (containing about 3×10^4 alveolar sacs) is effectively the smallest unit of gas exchange in the normal lung. New generation PET scanners are now being built with a higher sensitivity (25 fold) and increased resolution (~4 mm FWHM) to cover a transaxial distance of 24 cm.

Scanning times can be reduced to around 5 s, if a rapid response is required. Inevitably, counts will be at a premium with such short scan times. Nevertheless, large quantities (>2,000 MBq) of a positron emitter, such as $C^{15}O$, can be given without excessive radiation exposure to the subject, because of its short half-life (122.6 s).

Regional lung structure

A unique feature of PET is its ability to distinguish the fraction of blood, tissue and gas contained in each lung voxel (volume imaging element). For this, two measurements need to be made: 1) a lung density (D_L) scan; and 2) a vascular volume ($C^{15}O$) scan. As mentioned previously, the transmission scan provides the measurement of D_L.

Vascular volume

Regional blood volume (mL blood·mL^{-1} thorax) is measured after a 4 min open circuit inhalation of tracer quantities of ^{11}CO or, more usually, $C^{15}O$ ($1{,}500\times10^6$ Bq·min^{-1}) [4]. This combines with haemoglobin in the red blood cells of the pulmonary capillaries to form ^{15}O-carboxyhaemoglobin. During the subsequent 6 min scan, four peripheral venous blood samples are taken for the measurement of vascular radioactivity. In any region, the vascular volume per mL thoracic volume (rV_V) is:

$$rV_V = DC \times r[C^{15}O]/(b[C^{15}O] \times K_E \times 0.9) \quad (1)$$

where DC is a decay correction factor for the scan counts, $r[C^{15}O]$ represents the $C^{15}O$ counts per voxel or group of voxels per second in a given lung region (r) after attenuation correction (fig. 2b), $b[C^{15}O]$ is the mean radioactive concentration (Bq·mL^{-1}) of the peripheral blood samples (measured using a NaI well counter), K_E is a cross calibration factor relating lung voxel counts to isotope concentration (Bq·mL^{-1}), and 0.9 is a correction factor for the peripheral lung haematocrit [6].

The vascular volume scan plays an important role in the derivation of extravascular tracer concentrations. For example, in a metabolic study using ^{18}F-deoxyglucose (^{18}FDG), the contribution of intravascular ^{18}FDG to the total voxel ^{18}FDG can be calculated from the instantaneous ^{18}FDG concentration in a peripheral blood sample ($b[^{18}FDG]$) and the voxel vascular volume (rV_V):

$$r[^{18}FDG]_{EV} = r[^{18}FDG]_{tot} - (b[^{18}FDG] \times rV_V \times K_E) \quad (2)$$

where EV and tot refer to ^{18}FDG isotope concentrations in the extravascular and total voxel compartments, respectively.

In the heart chambers, the measured values for rV_V range from 0.9–0.95 mL blood·mL^{-1} thorax [7]; the small difference between these and unity being caused by the spatial resolution of the tomograph and cardiac movement. This measurement constitutes the "recovery coefficient", which can be used to determine "mixed venous" concentrations of tracers subsequently administered and "sampled" with a region of interest situated over the right ventricular (RV) cavity.

Haematocrit

Using sequential red cell (^{11}CO-Hb) and plasma (^{11}C-methyl albumin) markers, the haematocrit of peripheral lung and the heart cavities (as a ratio of peripheral venous blood) has been measured, and was found to be 0.9±0.014 and 1.00±0.003, respectively [6]. To the extent that 70% of the pulmonary blood in the field of view is in large vessels with a normal haematocrit, the haematocrit in the pulmonary capillaries must be about 0.6 of that in peripheral venous blood. This would be consistent with the Fåhreus-Lindqvist effect. This haematocrit correction is incorporated into Equation (1), since it is not practicable to label both red cells and plasma in every study.

With ^{68}Ga-transferrin as a plasma marker, peripheral lung haematocrit in anaesthetized dogs was found to be the same as the large vessel haematocrit [8]. The discrepancy between dogs and humans may be due to the fact that the region of interest in the dog includes more large vessels.

Combined vascular and extravascular volume

The volume of gas-free lung per mL of thorax (V_{V+EV}) can be derived from measurements of total lung density (D_L) (fig. 2a) using: 1) the transmission scan [4]; or 2) the distribution volume of $H_2{}^{15}O$ (V_{TLW}) obtained by scanning 3–4 min after its intravenous injection to allow equilibration [8–10]. V_{V+EV} is related to D_L and V_{TLW} by the factors 1.04 (density of lung) and 0.82 (water fraction of lung), respectively. The calculations are made as follows:

$$\text{a)} \qquad rV_{V+EV} = (Tr_{(lung)}/Tr_{(LV)}) \times 1.019 \quad (3)$$

where Tr refers to the counts from the transmission scan using the ^{68}Ga/^{68}Ga ring source, for the lung and the left ventricular cavity (LV), and 1.019 is the ratio between

blood and lung densities (1.06/1.04). The transmission scan counts from the left ventricular chamber are used as a normalizing factor of known vascular density.

$$\text{b)}\quad r\dot{V}_{V+EV} = 1.03 \times r[H_2{}^{15}O] \,/ \int_{T_1}^{T_2} b[H_2{}^{15}O](t)\, dt \qquad (4)$$

where $r[H_2{}^{15}O]$ is the integrated count for the duration of the scan (T_1 to T_2), $b[H_2{}^{15}O](t)$ is the blood concentration of radioactivity ($Bq \cdot mL^{-1}$) as a function of time, and 1.03 is the ratio of blood water to tissue water (0.84/0.82).

Extravascular tissue volume and alveolar gas volume

$r\dot{V}_{EV}$ is obtained by the subtraction of $r\dot{V}_V$ from $r\dot{V}_{V+EV}$. Extravascular density (D_{EV}; used in previous publications [4, 11] (fig. 2c)) equals $\dot{V}_{EV} \times 1.04$. $\dot{V}_{EV}$ (or D_{EV}) is affected by total thoracic expansion (*i.e.* V_{tot} or $V_{V+EV+Alv}$), since lung density (D_L) is proportional to $1/V_{tot}$. The biggest component of V_{tot} (about 75%) is alveolar gas volume (V_A).

$$r\dot{V}_A = 1 - rD_L/1.04 \qquad (5)$$

where 1.04 is the density of gas-free lung tissue, including blood.

In any condition associated with airflow obstruction, V_A will increase and, as a consequence, $\dot{V}_{EV}$ will tend to fall. There appears to be a natural variation of $\dot{V}_{EV}$, which is dependent on the size of the subject - taller people having greater lung expansion and lower $\dot{V}_{EV}$. BRUDIN and co-workers [11] proposed a correction (called the Expansion Index) based on body height and the number of voxels in a right lung section at mid-heart level in a series of normal subjects. This index was applied to patients with chronic airflow obstruction [12], to assess the contribution of hyperinflation alone on $\dot{V}_{EV}$.

To what extent does $\dot{V}_{EV}$ (extravascular tissue volume·mL^{-1} thorax) reflect the tissue volume of the acinus (alveolar sacs and ducts, and respiratory bronchioles) alone? Each millilitre of thoracic volume includes extra-acinar structures, *i.e.* the volume of arteries, veins, bronchi and bronchioles, which contribute 10–18% to the total. In calculating $\dot{V}_{EV}$, the large blood vessel volume component is "removed" from the density value of a given volume element, thus resulting in an underestimation of parenchymal $\dot{V}_{EV}$ due to the remaining "holes". A correction to account for this has been proposed [11], which provides a better estimate of the true "alveolar" tissue concentration, by normalizing $\dot{V}_{EV}$ to the reduced tissue occupancy of the thoracic volume element, *i.e.*:

$$\dot{V}_{EV,alv} = \frac{\dot{V}_{EV}}{1 - fec\dot{V}_V} \qquad (6)$$

where f_{ec}, the fraction of $\dot{V}_V$ associated with extracapillary vessels, has been assigned a value of 0.75. Therefore, the "gas exchanging" or "alveolar" tissue concentration ($\dot{V}_{EV,alv}$) has a value some 15% greater than $\dot{V}_{EV}$. This correction was introduced in terms of density by BRUDIN and co-workers [11] as $D_{EV,alv}$.

Alveolar (or acinar) expansion

The ratio of gas volume to alveolar tissue concentration ($V_A/\dot{V}_{EV,alv}$; mL gas·mL^{-1} alveolar tissue) can be used to calculate the expansion or gas volume of an individual alveolus (ψ_{alv}; mL gas·$alveolus^{-1}$) if the tissue content of the alveolus is known (k_{alv}; mL tissue·$alveolus^{-1}$), *i.e.*:

$$\psi_{alv} = \frac{V_A}{\dot{V}_{EV,alv}} \times k_{alv} \qquad (7)$$

k_{alv} has a value of the order of 2 µml $alveolus^{-1}$, but is clearly not known quantitatively for a given individual. However, a measure of the relative alveolar expansion (V_{alv}; mL gas·mL^{-1} tissue) can be determined as:

$$V_{alv} = \frac{\psi_{alv}}{k_{alv}} = \frac{V_A}{\dot{V}_{EV,alv}} \qquad (8)$$

This parameter, which was previously referred to as "alveolar size" by BRUDIN and co-workers [11], can be used to quantify the regional differences in alveolar expansion if a reasonable degree of homogeneity of interstitial fluid and alveolar structure exists throughout the lung. In normal subjects, there is quite a pronounced ventral to dorsal gradient of acinar expansion (table 2), which confirms the well-known vertical gradients of regional lung expansion and alveolar size. However, it is likely that $V_A/\dot{V}_{EV,alv}$ has no physiological meaning in abnormal lungs, because of the structural disorganization of tissue.

Table 2. – Compartmental analysis of regional differences in lung structure using PET in normal subjects (n=5) [4] and in anaesthetized dogs (n=13) [10], in supine posture

	Ventral	Dorsal	Ratio Ventral/Dorsal
$\dot{V}_V$ mL·mL^{-1} thorax	0.075 (0.094)	0.21 (0.2)	0.36 (0.47)
$\dot{V}_{EV}$ mL·mL^{-1} thorax	0.11 (0.15)	0.15 (0.2)	0.75 (0.76)
$\dot{V}_{EV}/\dot{V}_V$ mL·mL^{-1}	1.47 (1.6)	0.72 (0.98)	2.04 (1.63)
V_A mL·mL^{-1} thorax	0.82 (0.76)	0.64 (0.6)	1.28 (1.27)
$V_A/\dot{V}_{EV,alv}$ mL·mL^{-1}	7.04 (4.7)	3.59 (2.55)	1.96 (1.85)

Data for anaesthetized dogs are presented in parenthesis. $\dot{V}_V$: vascular volume; $\dot{V}_{EV}$: extravascular volume; $\dot{V}_E/\dot{V}_V$: extravascular/vascular volume ratio; V_A: alveolar gas volume; $V_A/\dot{V}_{EV,alv}$: alveolar gas/alveolar tissue concentration ratio, "acinar expansion"; PET: positron emission tomography.

Table 2 compares structural parameters, derived from measurements of rV_V and V_{V+EV}, in awake supine normal subjects [4] and anaesthetized supine dogs [10]. Considering the biological differences and the fact that rV_{V+EV} was measured by $^{68}Ge/^{68}Ga$ transmission scanning in one study and by $H_2{}^{15}O$ scanning in the other, the agreement is remarkable. Both dogs and humans show vertical gradients, increasing from ventral to dorsal, which are more pronounced for vascular volume than for extravascular volume. There are gradients in the reverse direction (ventral values exceeding dorsal) for regional gas volume and acinar expansion. $V_{EV,alv}$ reflects the density of individual gas exchange units.

Regional ventilation, blood flow and gas exchange

Regional ventilation

Regional ventilation has been measured during the continuous inhalation of neon-19 (^{19}Ne: half-life ($T_{1/2}$) 17 s) [13, 14]; the theory and practice is similar to that used for krypton-81m ($T_{1/2}$ 13 s) [15]:

$$r(V'_A/V_A) = \lambda / (i[^{19}Ne]/r[^{19}Ne]_{alv} - 1) \quad (9)$$

where λ is the decay constant (2.39 min^{-1}) of ^{19}Ne, r(V'_A/V_A) is regional ventilation per millilitre alveolar gas volume, i[^{19}Ne] and r[^{19}Ne]$_{alv}$ are the inspired and regional alveolar concentrations of ^{19}Ne. The term r[^{19}Ne]$_{alv}$ is calculated as the voxel count rate for ^{19}Ne in the steady-state (MBq·mL^{-1} thorax) divided by rV_A. If V'_A/V_A is multiplied by V_A/V_{EV}, ventilation per acinar or per millilitre alveolar tissue is obtained (V'_A/V_{EV}) [12]. VALIND and co-workers [14] have shown, using a computer simulation, that in the normal range for V'_A/V_A (1.0–3.3 mL·min^{-1}·mL^{-1}) errors of -3 to +8% at the low and high end of the scale, respectively, may occur with the use of ^{19}Ne and PET. This arises mainly from the reinspiration of common dead space gas and by the decay of ^{19}Ne, with its short half-life, through the bronchial tree. In a further analysis, VALIND and co-workers [16] focused on the inhomogeneity of ventilation within a single volume element. In general, the volume-weighted average local ventilation can be assessed quite accurately from the mean local ^{19}Ne concentration when ventilation is distributed with a Gaussian frequency function. However, a bimodal distribution with normally ventilated units coexisting with low V'_A/V_A (<1.0 mL·min^{-1}·mL^{-1}) units resulted in underestimations of up to 60% in the computer simulations. This highlights a common problem with the steady-state method, because of the nonlinearity of the signal with flow.

Ventilation/perfusion ratios

Regional ventilation/perfusion ratios (V'_A/Q') have been assessed during the continuous intravenous infusion of ^{13}N in solution [7, 17], using the steady-state mass balance equation:

$$rQ' \times Cv = (rV'_A \times rC_A) + (\alpha_{N_2} \times rQ' \times rC_A) \quad (10)$$

where Cv and rC_A are the mixed venous and regional alveolar gas concentrations of ^{13}N, respectively. These data are obtained from a 7 min emission scan, recorded 5 min after the start of a 12 min constant infusion of 1,000 MBq of ^{13}N dissolved in saline. rC_A is calculated by dividing the ^{13}N voxel counts (MBq·mL^{-1} thorax) by rV_A, *i.e.* (1 - rD_L/1.04). Rearrangement of Equation (10) gives:

$$r(V'_A/Q') = (Cv/rC_A) - \alpha_{N_2} = \frac{RV[^{13}N]}{\{r[^{13}N]_{EV}/(1-rD_L/1.04)\}} - \alpha_{N_2} \quad (11)$$

where RV[^{13}N] is the radioisotope concentration in the right ventricular cavity (corrected for the recovery coefficient), r[^{13}N]$_{EV}$ is the recorded regional voxel count rate minus the ^{13}N counts calculated to arise from the arterial blood in the voxel element (equivalent to 0.4 × rV_V × RV[^{13}N]), and α_{N_2} is the blood:gas partition coefficient (mL·mL^{-1}) for nitrogen (α_{N_2} = 0.015 at 37°C).

RHODES *et al*. [17] considered the reinspiration of the common dead space gas on r[^{13}N]$_{EV}$ in some detail. This effect means that PET imaging measures "effective" local V'_A/Q' ratios rather than a V'_A/Q' ratio determined solely by bulk flow ventilation. This is particularly noticeable with high V'_A/Q' ratios. For example, at a bulk flow V'_A/Q' of 10, r[^{13}N]$_{EV}$ would measure an "effective" V'_A/Q' of 3.2. However, reinspiration of the common dead space has a similar effect on the physiological gases, such as oxygen and CO_2, which would have "effective" V'_A/Q' ratios of 4.7 and 8.0, respectively, the differences between the gases being due to their different solubilities in blood. At low and normal V'_A/Q' the discrepancies are negligible.

In eight out of 12 normal subjects [7], there was a small but systematic ventral to dorsal fall in V'_A/Q' ratio averaging 0.39 in absolute units. Mean V'_A/Q' for a single slice of the right lung was 0.8±0.23 (SD). Seven of the subjects showed discrete regions of very low V'_A/Q' at the dorsal border of the lungs, possibly due to airway closure brought on by the prolonged supine position.

In subjects with chronic airflow obstruction, failure to achieve a steady-state within 5 min of the start of the ^{13}N infusion may occur, because of low regional ventilation [18]. This happens because the exponential rate constant for equilibration ($V'_A/V_A + \alpha_{N_2} \times Q'/V_A$) is normally dominated by ventilation. The result of a low regional ventilation is to underestimate r[^{13}N]$_{EV}$ and overestimate V'_A/Q', unless corrections are made using the measured values of V'_A/V_A

Regional pulmonary blood flow

The practice at Hammersmith is to compute Q'/V_A region by region as r(V'_A/V_A)/r(V'_A/Q') [19]. V'_A/V_{EV} may be substituted to give Q' per millilitre extravascular tissue (or per "acinus"). This derivation of regional blood flow (a "free" measurement) compounds the errors inherent in the measurements of regional ventilation and (V'_A/Q'). A comprehensive analysis of the errors associated with these measurements has been made previously [18].

Alternative methods to measure Q' have, unfortunately, involved continuous pulmonary artery sampling [20], which rather precludes much clinical application. Albumin microspheres have been labelled with ^{68}Ga [21] and ^{11}C [22], but no pulmonary measurements have been reported, and pulmonary arterial sampling would be required to obtain absolute values. $H_2{}^{15}O$ infusion has been used in anaesthetized dogs [20], but the procedure is too complex and invasive for human use. The lung fields are scanned for 15 s during a 20 s central venous infusion of $H_2{}^{15}O$. The pulmonary input function is measured by blood withdrawal from a pulmonary artery catheter; a second PET scan (2–7 min later) measures the equilibrium distribution of $H_2{}^{15}O$.

However, this move towards dynamic methods avoids the errors associated with the nonlinearity of the steady-state model, and makes better use of the radioactivity administered to the subject. The increased sensitivity and spatial resolution of the new generation scanners should allow a better noninvasive measurement of the pulmonary input function by applying regions of interest to the right ventricle or pulmonary artery. An alternative to the *i.v.* infusion of $H_2{}^{15}O$ would be the inhalation of $C^{15}O_2$ and measurement of its subsequent rate of clearance to provide values of regional lung perfusion, as previously described by WEST *et al.* [23].

Structure-function relationships

Normal subjects

BRUDIN and co-workers [19, 24] have explored the relationships between the volume elements within the voxel (gas, blood and tissue) and ventilation and blood flow.

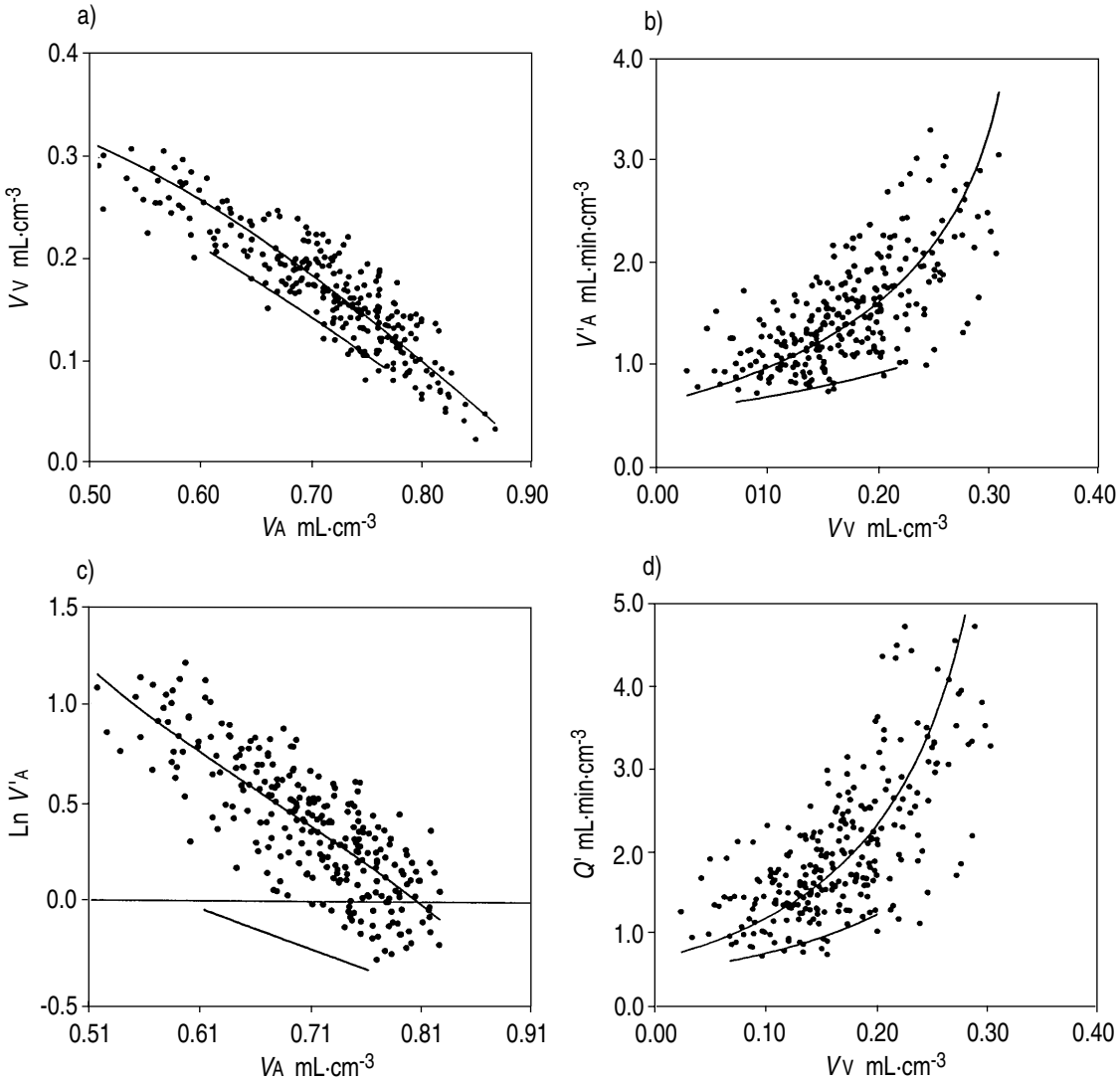

Fig 3. – Relationships between structural and functional parameters in normal subjects studied supine with a single plane scanner. Parametric images of alveolar (V_A) and vascular (V_V) volume, and alveolar ventilation (V'_A) were obtained by transmission, ^{11}CO and ^{19}Ne scanning, respectively, (see text). Blood flow (Q') was obtained indirectly from the regional measurements of V'_A/Q' (obtained using ^{13}N infusion) and V'_A. Regional values of each parameter were determined by averaging pixels in 1.3 cm^2 areas drawn within the right lung field. (The number of regions varied between 25 and 44 for each of the eight subjects). Continuous lines represent functions derived from the group averaged parametric relationships obtained for individuals [19, 24], supine (longer lines) and one subject studied prone (shorter lines). Redrawn from [19, 24] with permission.

They found the expected vertical gradients for all parameters, and that central to peripheral gradients at the same horizontal level were insignificant. One must remember that the identification of gradients and the presence or absence of inhomogeneity may be hindered by the relatively poor spatial resolution of PET. Nevertheless, when all regions of interest (drawn as 1.3 cm squares - slice thickness ~1.8 cm) were analysed, irrespective of their anatomical location, some interesting correlations emerged.

Firstly, there was a significant linear correlation between rV_A and ln(rV'_A) (fig. 3c) [24]. When the number of alveolar units in the region of interest (ROI) was taken into account, by dividing by V_{EV}, there was a significant linear relationship between V'_A/V_{EV} and V_A/V_{EV}. This is compatible with the exponential shape of the static pressure volume curve of individual alveolar units, first proposed by SALAZAR and KNOWLES [25]. It also supports the notion of MILIC-EMILI *et al*. [26] that the elastic properties of the alveoli are the major determinants of the distribution of ventilation during quiet breathing.

Secondly, there was an inverse correlation between regional vascular and alveolar gas volumes (fig. 3a). This observation prompted the notion of a "competition for space" within the voxel element [24]. For example, alveoli in voxels in the ventral part of the supine lung or in the cranial portion of the upright lung are subject to higher distending pressures than alveolar units elsewhere. This, plus the effect of gravity in reducing vascular volumes in the superior parts of the lung, means an increase in gas volume within the voxel. In terms of the ventral to dorsal gradient, the decrease in rV_A is mostly offset by an increase in rV_V (fig. 3a), since the increases in V_{EV} are smaller (table 2). This implies that vascular volume is inversely related to alveolar expansion (V_A/V_{EV}), which in itself is a determinant of regional ventilation.

It has long been known that the vertical gradients of pleural surface pressure and alveolar expansion are related to the lung weight subtended by a given horizontal lung plane [27]. BRUDIN and co-workers [24] calculated that the gradient of blood volume from ventral to dorsal lung regions accounted for three quarters of the gradient of diminishing alveolar size - one half being linked to the gradient of V_{EV} itself, because of the blood weight, and one quarter being explained by "competition for voxel space". The implication, which needs to be tested further, is that the vertical vascular gradient, by virtue of its mass and volume, is the major determinant of the gradient of alveolar size and, hence, of the gradient of regional ventilation. Figure 3b shows the correlation between regional vascular volume and regional ventilation [24].

Lastly, regional blood flow increases in a hyperbolic manner as vascular volume increases (fig. 3d) [19]. Thus, there is a mechanical link between the gradients of blood flow and ventilation *via* vascular volume and mass on the one hand, and alveolar size on the other. This may explain why Q' and V'_A/V_A are well-matched in the vertical axis in the supine posture, leaving only a small V'_A/Q' gradient (table 3) [7, 19].

These results demonstrate the usefulness of comparisons between functional and structural information. This results from the ability of PET to provide quantitative measurements of isotope concentration, density and gas volume within well-defined regions of the lung, non-invasively, during normal breathing.

Chronic airflow obstruction

Differences in structural and functional parameters for a whole right lung slice (rather than gradients within the slice) between normal subjects and patients with various types of airflow obstruction are shown in table 3. In a study of 15 nonsmoking and 15 smoking subjects [11], the only significant difference was 14% higher extravascular volume (V_{EV}) in smokers, increasing to 21% if their hyperexpansion (E) was taken into account (normalized extravascular volume). This may reflect some inflammatory change. The smokers as a group had 4–10% lower values (as percentage predicted) of forced expiratory volume in one second (FEV_1) vital capacity (VC), transfer factor of the lungs for carbon monoxide ($T_{L,CO}$) and carbon monoxide transfer coefficient (K_{CO}) than the nonsmoking group. On an individual basis, taking both groups together, V_{EV} had a negative correlation with $T_{L,CO}$, and vascular volume (V_V) was positively correlated with K_{CO}. The expansion index (E) was linked with smoking history and with reductions in FEV1 and VC [11].

There were distinctive patterns associated with an emphysematous (type A) and bronchitic (type B) clinical classification [12] - the K_{CO} being the main distinguishing feature (averaging 39% in type A and 81% in type B), although airflow obstruction was also more severe in type A. The most poorly ventilated regions tended to have a low V_{EV} and high V'_A/Q' in the emphysematous patients, and a high or normal V_{EV} and a low V'_A/Q' in the bronchitic patients [12]. These high and low V'_A/Q' patterns are consistent with the findings in these two groups using the multiple inert gas elimination technique [28]. Although mean V'_A/Q' could be normal in type A patients, the standard deviation was always increased. Blood flow per alveolus (*i.e*. per mL tissue) was lower in emphysema than in bronchitis - not unexpectedly in view of the alveolar destruction shown on histopathology, and supported by the low density on X-ray CT scanning [12]. For both groups together, the $V_{EV}/[V'_A/Q']$ ratio (a mixed structural/functional index) correlated well with K_{CO}. These differences between type A and type B patients support the notion that bronchial inflammation or oedema predominate in some cases of chronic obstructive lung disease; whereas, alveolar destruction is the major feature of others.

Not surprisingly, the structure-function pattern in chronic asthma resembles bronchitis more than emphysema. In 10 asthmatic patients (Brudin LH, unpublished) there was a tendency for V_{EV} (normalized for hyperexpansion) to be high, consistent with an inflammatory infiltrate. As in the type B patients, low values of $r[V'_A/Q']$ were associated with low $r[V'_A/V_A]$ (table 3).

Table 3. – PET measurements of regional lung structure and function in normal subjects and patients with different types of airflow obstruction, all studied in supine posture

	Normals [11]	Smokers [11]	Asthma [*]	Bronchitis (Type B) [12]	Emphysema (Type A) [12]
Subjects n	15	15	10	4	4
V_{EV} mL·mL^{-1} thorax	0.10 (0.02)	0.11 (0.03)	0.09–0.10	0.11–0.13	0.04–0.11
Expansion ratio	1.00	1.12	1.39	1.5–2.7	1.6–2.0
Normalized V_{EV} mL·mL^{-1}	0.10 (0.015)	0.12 (0.022)	0.08–0.23	0.13–0.24	0.07–0.17
V_V mL·mL^{-1} thorax	0.16 (0.02)	0.16 (0.03)	0.10–0.16	0.08–0.14	0.06–0.11
Subjects n	8	9			
Ventilation per alveolus mL·min·mL^{-1} lung	13.8 (6.7)	10.9 (4.4)	2.6–12.1	5.3–12.7	9.4–22.7
Perfusion per alveolus mL·min·mL^{-1} lung	17.8 (8.0)	17.4 (7.2)	5.5–13.2	12.1–19.1	7.7–14.8
V'_A/Q'	0.81 (0.14)	0.66 (0.12)	0.35–1.31	0.4–0.86	0.76–2.92
SD (V'_A/Q')	0.15 (0.05)	0.13 (0.04)	0.13–0.36	0.13–0.27	0.34–0.61

Values are presented as mean, and SD in parenthesis for sections at the mid-heart level in the right lung. V'_A/Q': alveolar ventilation/perfusion ratio. For further abbreviations see legend to table 2. Taken from [11] and [12] as indicated (*: L.H. Brudin, unpublished); Type A, Type B: clinical classification [12].

Interstitial lung disease

Regional vascular and extravascular volumes in sarcoidosis and cryptogenic fibrosing alveolitis (CFA) depend upon the activity of the disease and the extent of fibrosis. There is also a sampling problem if only one or two transaxial slices are examined, and mean values may mask intraregional inhomogeneity. Regional vascular volumes were reduced in CFA [29, 30], particularly if the disease was "active", in keeping with low values for lung transfer factor ($T_{L,CO}$) [31]. In sarcoidosis, where $T_{L,CO}$ tended to be higher, normal values of rV_V were frequently found [32], but low values did occur [29]. In both sarcoidosis and CFA V_{EV} is considerably increased, up to 200% of the predicted value [29–32]. In "active" interstitial lung disease, defined as clinical, radiological or functional deterioration, or with a recent lung biopsy showing alveolar or interstitial inflammation, vascular permeability (see below) was increased compared to "inactive" disease (clinical and function stability) [31] (table 4). Regional glucose metabolism, as an index of inflammatory activity (see below), increased in interstitial lung disease, more so in sarcoidosis [32] than in CFA [30].

Pulmonary vascular disease

In acute myocardial infarction with diffuse interstitial oedema, regional vascular volumes (rV_V) were normal but there was a generalized increase in regional lung density (D_L). Extravascular volumes (V_{EV}) were increased 50–60%, the ventral/dorsal (V/D) V_{EV} ratio was 0.95 (normal 0.87) [35]. In two patients with acute alveolar oedema, with patchy consolidation on chest radiographs, there was a reduction in rV_V in the dependent zones with a large increase in rV_{EV} (up to 0.85 mL·mL^{-1} thorax) [35]. In contrast, there is a marked reduction of rV_V in chronic pulmonary venous hypertension [36], especially in the dorsocaudal (dependent) regions (74% normal). rV_{EV} was increased generally, but more so dorsocaudally than ventrocaudally (151 and 130% of normal, respectively), resulting in a V/D ratio of 0.75. This decrease in rV_V and increase in dorsal rV_{EV} is thought to reflect vascular destruction on the one hand, and tissue proliferation and scarring on the other.

Table 4. – PET measurements of extravascular volume (V_{EV}) and vascular permeability (pulmonary transcapillary escape rate, (PTCER)) in clinical situations

		Subjects n	V_{EV} mL·mL^{-1}	PTCER 10^{-4}·min^{-1}
Normal subjects	[33]	8	0.17 (0.04)	21 (11)
Smokers	[34]	7	0.19 (0.04)	21 (14)
Congestive heart failure	[33]	6	0.3 (0.12)	44 (16)
ARDS	[33]	8	0.37 (0.4)	170 (79)
Pneumonia (infiltrate)	[33]	15	0.43 (0.15)	173 (99)
Pneumonia (unaffected)	[33]		0.14 (0.04)	90 (35)
Interstitial disease (active)	[31]	10	0.19 (0.09)	120 (40)
Interstitial disease (inactive)	[31]	6	0.21 (0.16)	32 (10)

Data are presented as mean, and SD in parenthesis. PET: positron emission tomography; ARDS: adult respiratory distress syndrome.

Vascular permeability

In the presence of leaky capillaries, certain radiolabelled tracer molecules injected intravenously will escape into the extravascular space of the lung, to be cleared either by back diffusion into the vascular space or, more slowly, by lymphatic flow. With large molecular weight tracers, such as plasma proteins, equilibrium between the vascular and extravascular spaces is reached quite slowly, even in "leaky" lungs, because the time constant (product of the capacitance of the interstitial space and the vascular diffusion resistance) is quite large. Therefore, the increase in radioactive counts over the thorax following tracer injection, as recorded by external detectors, is almost linear over the first 45 min. This slope, called the "protein leak index", is equivalent to a rate constant with units of time^{-1}, and is proportional to the vascular-permeability to surface-area product. As originally described, the plasma protein tracer was transferrin labelled with ^{113}Indium; at the same time, a nondiffusible intravascular tracer (red cells labelled with ^{99m}Tc) was injected intravenously, so that the instantaneous ^{113}In/^{99m}Tc ratio would reflect the proportion of the ^{113}In-transferrin which had left the vascular space [37]. Because of their different photon energies, both radioisotopes could be counted simultaneously. This method was pioneered by GORIN and co-workers [37], and validated against simultaneous measurements of protein flux in sheep [38]. GORIN and co-workers [37] analysed their data mathematically with forward and reverse rate constants (K_1 and k_2) between the vascular and extravascular compartments; K_1 divided by the plasma volume under the detector represents a surface area independent estimate of pulmonary vascular permeability.

With γ-cameras or single NaI scintillation detectors there are geometric problems, especially concerning the contribution of the chest wall. PET provides increased spatial and quantitative accuracy, as already discussed, but it cannot resolve simultaneously a diffusible and a nondiffusible tracer, because all positron emitters share the same 511 keV γ-energy. With a PET study of vascular permeability, the assumption is made: 1) that the distribution of the plasma protein tracer (^{68}Ga-labelled transferrin) at time zero (the time of the intravenous injection) is exclusively intravascular; and 2) that the vascular volume does not change throughout the study. The St Louis group, who have used the ^{68}Ga-transferrin method extensively [33, 34, 39–43], use the K_1, k_2 analysis [37] rather than the simple slope index of DAUBER *et al*. [44], deriving the pulmonary transcapillary escape rate (PTCER) as follows:

$$r[^{68}Ga] = rVpl \int_{T_1}^{T_2} pl[^{68}Ga](t)\, dt + K_1 \int_{T_1}^{T_2} pl[^{68}Ga](t) \; * \; e^{-k_2 t}\, dt \quad (12)$$

where r[^{68}Ga] is the regional ^{68}Ga-transferrin count (vascular and extravascular) for the nth PET scan (from time T_1 to T_2), pl[^{68}Ga](t) is the plasma concentration of ^{68}Ga in a peripheral blood sample at time t, rVpl is the regional plasma volume, and K_1 and k_2 are the forward and reverse transport rate constants for protein movement between the vascular and extravascular spaces. The asterisk represents the convolution operator. rVpl, K_1 and k_2 are calculated by an iterative parameter estimation technique. K_1 (determined regionally) is normalized to vascular surface area (assumed to be proportional to the local plasma volume, rVpl), giving:

$$rPTCER = K_1/rV_{pl} \quad (13)$$

where PTCER is the pulmonary transcapillary escape rate (per min^{-1}).

MINTUN and co-workers [40] have presented a careful error analysis of these two analytical methods. Both depend upon the leaky parts of the lung being adequately perfused. The slope index method, although less rigorous than the PET technique, can give useful clinical information [45], and has proved sensitive and specific for lung injury (*versus* hydrostatic oedema) in controlled animal models [44].

The St Louis group have obtained interesting data in experimental models and in a variety of clinical conditions. In a canine model of local or diffuse oleic acid lung injury, rPTCER correlated well with the volume of interstitial oedema in perivascular and peribronchial cuffs, but the correlation with light and electron microscopic evidence of alveolar damage broke down at the higher levels of rPTCER (>700 $\times 10^{-4}$·min^{-1}) [42].

The clinical results obtained by the St Louis group are set out in table 4. Unlike the ^{99m}Tc-diethylenetriamine penta-acetate (DTPA) aerosol measurement of epithelial membrane clearance, the intravenous ^{68}Ga-transferrin exchange through the endothelium is not abnormal in smokers [34]; this means that a history of smoking is not a confounding issue in the interpretation of PTCER values. The method seems to be specific, judging by the normal values in congestive heart failure in the presence of an increase in extravascular volume (V_{EV}) [33]. Raised values of PTCER in unaffected areas in patients with pneumonia [33], and in active interstitial lung disease [31] are intriguing, because of the absence of pulmonary oedema judging from the normal values of V_{EV}. Future developments in this area are likely to include the use of smaller molecules of differing size (DTPA and inulin for example) in an attempt to improve the sensitivity of this approach to more subtle changes in microvascular integrity [46].

Receptor binding

Beta-adrenergic receptor binding

The first attempts to image intrathoracic β-adrenergic receptors (β-ARs) in animal models using gamma-cameras and iodine-labelled radioligands were only partially successful [47, 48]. Nonspecific binding was >40% of the signal and no quantification of binding capacity *in vivo* was possible. PET studies of β-AR imaging were initiated by the Orsay PET group using the

ligand CGP-12177 labelled with carbon-11 [49]. They developed a double injection method in a dog model with a high specific activity *i.v.* injection (1.2 µg in 111 MBq), followed 30 min later by a low specific activity dose (11–27 µg in 370 MBq), and a graphical approach, from which the β-AR binding capacity (Bmax) was derived. Their interest was confined to the myocardium [49]. CGP-12177 was an extremely good choice of ligand for PET receptor binding studies for several reasons: 1) high binding affinity (K_D <0.4 nM); 2) low nonspecific binding (<10%); 3) slow *in vivo* metabolism; and 4) amenable to labelling with carbon-11.

Studies on cell populations *in vitro* had shown that CGP-12177 bound only to cell surface receptors, unlike lipophilic ligands, such as dihydroalprenolol [50]. *In vivo* studies using the tritiated form ([^{3}H]-CGP-12177), showed rapid uptake in the rat with a tissue-plasma ratio of 153 for the lung 15 min after intravenous injection [51]. This ratio fell to 7.1 after prior blocking dose of unlabelled CGP-12177 (equivalent to a nonspecific binding fraction 4.6%). To achieve the optimal signal-to-noise ratio for PET, the active (*S*) enantiomer had to be labelled. This was achieved by asymmetric synthesis of the *S*-diamino precursor [52], which was reacted in turn with ^{11}C-phosgene to give *S*-[^{11}C]-CGP-12177. Metabolite studies showed that one hour after *i.v.* injection, more than 97% of the plasma radioactivity in the dog [53], and in humans [54], was unchanged *S*-CGP-12177. This was important, since PET measures ^{11}C indiscriminately.

This painstaking preliminary work paid dividends, because extremely good lung and myocardial signals were obtained (fig. 2d) in spite of the low density of lung tissue. The method of Delforge was modified to allow for vascular [^{11}C]-CGP-12177 in tissue and V_{EV} was used to express receptor density per mL extravascular tissue (fig. 2e). The total amount of cold CGP-12177 in both injections was taken into account in the calculation of Bmax. Consistent values were obtained in the normal human lung. Bmax for pulmonary β-ARs was 14.7±0.7 (SD) pmol·g^{-1} lung tissue [55], comparing well with *in vitro* measurements using [^{125}I]CYP for human lung slices (12.6–8.6 pmol·g^{-1} [56]) or lung membranes (23.5±2.6 pmol·g^{-1} [57]). No differences in Bmax were found between right and left lung, nor between central and peripheral regions [55]. Propranolol (20 mg *i.v.*) blocked the uptake of [^{11}C]-CGP-12177 (lung tissue/plasma ratio fell from 108 to 6.2), demonstrating that CGP-12177 binds to beta-receptors in humans with less than 10% nonspecific binding (fig. 2f). In normal subjects, 2 weeks dosing with oral and inhaled salbutamol significantly reduced pulmonary β-AR Bmax by 23% [58]. In the same subjects, the percentage reduction in lung β-AR Bmax correlated with the percentage reduction in peripheral lymphocyte β-AR Bmax [59]. This supports the use of peripheral lymphocytes as a surrogate for alterations in lung β-AR density. The scene is now set for double studies of up- and down-regulation of beta-receptor numbers in asthmatic subjects in response to the chronic administration of corticosteroid and β-agonist drugs.

Angiotensin converting enzyme activity

Although not strictly receptor binding, interest has been shown in the measurement of angiotensin converting enzyme (ACE), which is present in high concentrations in the lung. This enzyme is mainly situated on the luminal side of the pulmonary endothelium, where it catalyses the reaction of angiotensin I to the vasoactive compound angiotensin II, and is, therefore, thought to be a good indicator of endothelial integrity. Consequently, a derivative of the ACE inhibitor captopril (2-D-methyl-3-mercapto-propanoyl-L-proline) has been labelled with fluorine-18 (^{18}FCAP) by HWANG *et al*. [60].

Measurement of the biodistribution of ^{18}FCAP in the rat showed high uptake in the lung, kidney and aorta at 30 min (24, 3.2 and 1.4% injected dose per gram, respectively). When unlabelled FCAP was co-injected with ^{18}FCAP, doses of ~5 and 1 µg·kg^{-1} were required to reduce tracer uptake to 50% in the lung and kidney, respectively [60]. A displacement study performed on a normal subject showed the loss of over 50% of the activity from the lung during a 66 min period following the oral administration of 25 mg of FCAP 90 min after the injection of ^{18}FCAP, illustrating the feasibility of studies in humans. Details of the theory, error analysis, implementation and application have recently been published [61, 62].

Apart from some preliminary studies using ^{11}C-acetazolamide [63], which binds to the enzyme carbonic anhydrase, no other lung receptors have been investigated with PET. The Orsay group have imaged muscarinic receptors in the myocardium using ^{11}C-methylquinuclidinyl benzilate (MQNB) [64, 65].

Metabolic studies

Glucose metabolism

In PET imaging studies of the brain and heart, the use of ^{18}F-deoxyglucose (^{18}FDG) as a surrogate for glucose itself is well established [66]. After intravenous injection, ^{18}FDG is transported from blood across cell membranes as if it were glucose. It is then phosphorylated by the enzyme hexokinase, but is not metabolized further. Therefore, deoxyglucose-6-phosphate builds up in the tissue at a rate which reflects glucose metabolism.

To measure the metabolic rate for glucose, 111–185 MBq of ^{18}FDG is injected intravenously, followed by six 3 min and nine 5 min serial PET scans. Peripheral venous blood is sampled throughout for pl[^{18}FDG]. For each scan, the extravascular tissue concentration, r[^{18}FDG]$_{EV}$, for each ROI, is obtained by subtracting intravascular ^{18}FDG, using Equation (2). r[^{18}FDG]$_{EV}$ is made up to two components, free (f) ^{18}FDG and metabolized (m) ^{18}FDG. Free ^{18}FDG is in equilibrium with plasma ^{18}FDG at times (t) >5 min, so that:

$$r[^{18}FDGf]_{EV}(t) = pl[^{18}FDG](t) \times V_{dis} \qquad (14)$$

where V_{dis} is the volume of distribution.

The metabolic accumulation of r[^{18}FDGm]$_{EV}(t)$ in any region of lung at time t is proportional to: 1) the whole blood concentration b[^{18}FDG]; 2) the arteriovenous extraction (E); and 3) the arrival (*i.e.* flow) of ^{18}FDG per mL thorax per minute (Q'). Integrating r[^{18}FDGm]$_{EV}(t)$ over short time intervals (Δt) to time T gives:

$$r[^{18}FDGm]_{EV}(T) = Q' \times E \int_0^T b[^{18}FDG](t)\ dt \quad (15)$$

Summing Equations (14) and (15) to give r[^{18}FDG]$_{EV}$(T) and dividing through by pl[^{18}FDG](T) gives:

$$\frac{r[^{18}FDG]_{EV}(T)}{pl[^{18}FDG](T)} = V_{dis} + Q' \times E \times \frac{\int_0^T b[^{18}FDG](t)\ dt}{pl[^{18}FDG](T)} \quad (16)$$

Plotting the tissue to plasma ratio (left hand, Equation (16)), against the ratio of integrated whole blood concentration to plasma concentration at various times, T, gives a linear function whose slope [$Q \times E$] represents the rate of ^{18}FDG uptake; the intercept is the extravascular distribution volume of free ^{18}FDG. This analysis is known as the Patlak plot [67]. The rate of ^{18}FDG uptake is conventionally expressed as mL·min^{-1}·mL^{-1} extra-vascular (EV) tissue by normalizing r[^{18}FDG]$_{EV}$(T) to V_{EV}.

There has been much interest in the high ^{18}FDG uptake in pulmonary neoplasms, where the tumour/contralateral lung uptake ratio was 6.6 (range 2.7–14.6) in one study [68], and 9.5±12.2 in another [69]. Figure 2h shows the high signal in the tumour and its draining nodes and the central necrosis in the tumour itself [68]. Other ways of quantifying the signal include the "differential uptake ratio" (DUR), which relates thoracic pixel counts to the injected dose (MBq per kg body weight) times a calibration factor [70, 71]; values of 5.55±2.8 [71] and 5.63±2.38 [70] for the tumour compared with 0.95±1.0 [71] and 0.56±0.27 [70] for uninvolved tissue. A less satisfactory quantitative index is the tumour to shoulder muscle ratio [72], which gives values of 4.4±2.2 for neoplastic and 1.5±0.3 for normal tissue.

NOLOP *et al*. [67] reported that there was no correlation between tumour type and rate of ^{18}FDG uptake, and that has been the subsequent experience. False positives occur with caseating granulomas (*e.g.* histoplasmosis) [71, 72], and false negatives have been seen with a small scar cancer (a 1 cm nodule) [71], carcinoid [69, 70], and a squamous carcinoma and liposarcoma [72]. The occurrence of false positives may be related to the involvement of white cells in these pathologies, and caution must be exercised when attempting to diagnose malignancy in the presence of possible inflammation (see below) and with the interpretation of changes during therapy. In general, the sensitivity and specificity for single pulmonary lesions is greater than 80% [71, 72]. ^{18}FDG uptake will probably prove very useful for assessing metastatic disease, either in the mediastinal lymph nodes [70], or more distant spread using whole-body imaging [69, 73].

Increased ^{18}FDG uptake has also been measured in experimental models of pulmonary inflammation in rabbits [74], in acute (pneumococcal instillation into the right upper lobe) and chronic (bleomycin instillation) situations. With the *Streptococcus pneumoniae* model, local ^{18}FDG uptake peaked at 15 h postinstillation at 6–19 times normal, returning to baseline 30 h later [74]. There was a smaller (2–4 fold) increase in glucose uptake after bleomycin, which took over 20 days to resolve.

The reason for the increased ^{18}FDG signal in inflammation is the presence of neutrophils, lymphocytes and macrophages. These cells have a high anaerobic to aerobic metabolic ratio because of a relative lack of oxidative enzymes. Compared to aerobic pathways, anaerobic metabolism consumes considerably more glucose to produce equivalent amounts of adenosine triphosphate (ATP). On autoradiography, using ^{3}H-deoxyglucose, positive staining was seen in neutrophils in the alveolar spaces (but not in other cells or in neutrophils in the alveolar septum) in experimental streptococcal pneumonia [74].

In humans, ^{18}FDG uptake has been measured in two chronic inflammatory conditions, sarcoidosis [32] and cryptogenic fibrosing alveolitis (CFA) [30]. In patients with sarcoidosis (n=7), the glucose metabolic rate averaged 4.1 (range 2.6–6.1) μmol·h^{-1}·mL^{-1} (EV) lung tissue (normal values 0.57–1.9 μmol·h^{-1}·mL^{-1}) with marked differences between regions and between right and left lungs (R/L ratio 0.76–2.04). Following treatment with corticosteroids (n=3), prednisolone 40 mg daily for 4 weeks and gradual reduction thereafter, there was a 58% (48–67%) reduction in the glucose metabolic rate, which was accompanied by a fall in serum ACE levels [32].

In CFA [30], glucose metabolism was only abnormal in 5 out of 9 patients studied; these values were lower than in sarcoidosis (2.3–3.9 μmol·h^{-1}·mL^{-1}) and changed little with immunosuppressive treatment. The patient with the highest value (3.9 μmol·h^{-1}·mL^{-1}) responded with a 38% fall after 12 months of therapy, accompanied by clinical and functional improvement.

Amine metabolism

One of the strengths of PET is that ^{11}C can be incorporated into molecules without altering their biological activity. For example, the amine ^{11}C-5-hydroxytryptamine (^{11}C-5HT) has been synthesized [75] and its first pass extraction has been measured in the lungs of healthy volunteers [76]; ^{11}CO-erythrocytes were used as the reference label. The first pass extraction (64±3.6%) was reduced (54±1.4%) if a competitive inhibitor (imipramine) was given beforehand. There is also a high single pass extraction of ^{11}C-chlorpromazine (90±5% in normal subjects (n=4) and 64±7% in patients with airflow obstruction (n=6)) [77].

The high extraction of these amines is to some extent due to their lipophilicity, but another factor is related to the need for the lung to remove and deactivate a number of endogenous vasoactive amines from the circulation, such as 5HT and norepinephrine, for which specific transport mechanisms and breakdown pathways (employing monoamine-oxidase) exist. These processes

require selective, energy-dependent transport systems across the pulmonary endothelial membrane, which makes them vulnerable to tissue injury or hypoxia. On the other hand, amines such as epinephrine and dopamine are not actively transported. A reduction in pulmonary amine uptake may, therefore, be a more sensitive and earlier indicator of endothelial malfunction than increased permeability to macromolecules. For example, in adult respiratory distress syndrome (ARDS) a decrease in pulmonary serotonin (5HT) extraction correlates with the severity of the disease [78].

Pharmacokinetics

The uptake of the carbon-11 labelled antibiotic, ^{11}C-erythromycin, has been measured in lobar pneumonia [79]. The mean extravascular concentrations, after correction for intravascular ^{11}C-erythromycin and expressed per mL V_{EV}, were 5.7±2.3 $\mu g \cdot mL^{-1}$ in the pneumonic lung and 6.9±2.3 $\mu g \cdot mL^{-1}$ in the contralateral (radiologically normal) lung. The ^{11}C-erythromycin was co-injected with 250 mg of unlabelled erythromycin lactobionate. The concentration of erythromycin (5.7 $\mu g \cdot mL^{-1}$ lung tissue) was well above the minimal inhibitory concentration for most sensitive bacterial species. Dynamic PET studies showed that an effective concentration of the antibiotic was reached within 10 min of injection, and was maintained throughout the period of measurement (60 min) [79].

This work with ^{11}C-erythromycin is a good example of the use of PET for the noninvasive measurement of tissue pharmacokinetics *in vivo*. Other studies, showing the high initial pulmonary extraction of ^{11}C-chlorpromazine [77] and ^{11}C-propranolol [80], illustrate how the lung can modulate the delivery of certain substances to the peripheral tissues. This in itself is relevant to a better understanding of drug pharmacokinetics and the future investigation of whole body drug distributions.

Future directions

The adaptation of positron emission tomography to the investigation of pulmonary function began relatively late, and has not developed with the same vigour seen with neurological and cardiological applications. Nevertheless, at its simplest, it has produced new physiological information with regard to the gas exchanging properties of the lung, in terms of the relationship between blood volume, alveolar size, ventilation and blood flow.

There has been a natural progression from the early assessment of "structural" parameters - blood, tissue, water and gas volumes - to the functional measurements of ventilation, blood flow and capillary leakage, and, more recently, on to investigations which have involved the measurement of metabolic and biochemical parameters, such as carbohydrate utilization, amine uptake and receptor binding.

A unifying aspect of previous investigations has been the ability of PET to provide quantitative *in vivo* measurements of the regional distribution of a wide ranging variety of physiological aspects of pulmonary function. The availability of suitable forms of positron emitting isotopes of carbon and fluorine provides the means to label a host of naturally occurring compounds and pharmaceuticals. Different functions can be measured on a regional basis for the same well-defined volume element. Above all, measurements made by external detection of the emitted 511 keV γ-rays - noninvasively and, if necessary, sequentially - are the crux of this methodology, providing a means to follow the time-course of lung diseases and the effect of therapy.

The lung is clearly an important metabolic organ, with control over the entire cardiac output; a role expressed dramatically by the almost total extraction of various substances having high biological activities. However, the future challenge will be in the quantification of the uptake of precursors of synthetic pathways, which may have quite small extraction fractions - as indicated by pilot work in the past using, for example, ^{11}C-palmitate to investigate surfactant production and ^{3}H-proline to assess the rate of collagen synthesis. Such measurements will inevitably need the increased sensitivity of the new generation scanners to enable adequate data sets to be obtained with acceptable radiation exposure levels. The increased spatial resolution of these new machines will, in addition, allow better definition of the mixed venous tracer input function, measured noninvasively by image "sampling" using a region of interest over the right ventricle. This should, in turn, allow a move away from the simple steady-state measurements towards the more robust protocols based on dynamic scanning and kinetic analysis.

Acknowledgements: The authors are grateful to P. Wollmer, S. Valind and L. Brudin for their collaboration and evaluation of unpublished data, and to T. Jones for constructive criticism of the manuscript.

References

1. Hughes JMB, Brudin LH, Valind SO, Rhodes CG. Positron emission tomography in the lung. *J Thorac Imag* 1985; 1: 78–88.
2. Valind SO, Wollmer P, Rhodes CG. Application of positron emission tomography in the lung. *In*: Reivich M, ed. Positron Emission Tomography. Allen R. Liss Inc., 1985; pp. 387–412.
3. Schuster DP. Positron emission tomography: theory and its application to the study of lung disease. *Am Rev Respir Dis* 1989; 139: 818–840.
4. Rhodes CG, Wollmer P, Fazio F, Jones T. Quantitative measurement of regional extravascular lung density using positron emission and transmission tomography. *J Comput Assist Tomogr* 1981; 5: 783–791.
5. Spinks TJ, Araujo LI, Rhodes CG, Hutton BF. Physical aspects of cardiac scanning with a block detector positron tomograph. *J Comput Assist Tomogr* 1991; 15: 893–904.
6. Brudin LH, Valind SO, Rhodes CG, Turton DR, Hughes JMB. Regional lung hematocrit in humans using positron emission tomography. *J Appl Physiol* 1986; 60: 1155–1163.

7. Rhodes CG, Valind SO, Brudin LH, *et al.* Quantification of regional V'/Q' ratios in humans by use of PET. II. Procedure and normal values. *J Appl Physiol* 1989; 66: 1905–1913.
8. Schuster DP, Mintun MA, Green MA, Ter-Pogossian MM. Regional lung water and hematocrit determined by positron emission tomography. *J Appl Physiol* 1985; 59: 860–868.
9. Schuster DP, Marklin GF, Mintun MA, Ter-Pogossian MM. PET measurement of regional lung density. *J Comput Assist Tomogr* 1986; 10: 723–729.
10. Schuster DP, Marklin GF, Mintun MA. Regional changes in extravascular lung water detected by positron emission tomography. *J Appl Physiol* 1986; 60: 1170–1178.
11. Brudin LH, Rhodes CG, Valind SO, Wollmer P, Hughes JMB. Regional lung density and blood volume in nonsmoking and smoking subjects measured by PET. *J Appl Physiol* 1987; 63: 1324–1334.
12. Brudin LH, Rhodes CG, Valind SO, Buckingham PD, Jones T, Hughes JMB. Regional structure-function correlations in chronic obstructive lung disease measured with positron emission tomography. *Thorax* 1992; 47: 914–921.
13. Crouzel C, Guenard H, Comar D, Soussaline F, Loc'h C, Plumer D. A new radioisotope for lung ventilation studies: 19-neon. *Eur J Nucl Med* 1980; 5: 431–434.
14. Valind SO, Rhodes CG, Jonson B. Quantification of regional ventilation in humans using a short-lived radiotracer: theoretical evaluation of the steady-state model. *J Nucl Med* 1987; 28: 1144–1154.
15. Fazio F, Jones T. Assessment of regional ventilation by continuous inhalation of radioactive krypton-81m. *Br Med J* 1975; 3: 673–676.
16. Valind SO, Rhodes CG, Brudin LH, Jones T. Measurements of regional ventilation and pulmonary gas volume: theory and error analysis with special reference to positron emission tomography. *J Nucl Med* 1991; 32: 1937–1944.
17. Rhodes CG, Valind SO, Brudin LH, Wollmer PE, Jones T, Hughes JMB. Quantification of regional *V'*/*Q'* ratios in humans by use of PET. I. Theory. *J Appl Physiol* 1989; 66: 1896–1904.
18. Brudin LH, Valind SO, Rhodes CG. Combined measurements of regional ventilation and *V'*/*Q'* ratio: correction for incomplete equilibration and error analysis of blood flow calculation. *Phys Med Biol* 1992; 37: 1077–1093.
19. Brudin LH, Rhodes CG, Valind SO, Jones T, Hughes JMB. Interrelationships between regional blood flow, blood volume, and ventilation in supine humans. *J Appl Physiol* 1994; 76: 1205–1210.
20. Mintun MA, Ter-Pogossian MM, Green MA, Lich LL, Schuster DP. Quantitative measurement of regional pulmonary blood flow with positron emission tomography. *J Appl Physiol* 1986; 60: 317–326.
21. Maguire B, Loc'h C, Steinberg M, Comar D. Stable labelling of serum albumin microspheres with Ga-68. *Int J Appl Radiat Isotop* 1986; 37: 360–361.
22. Turton DR, Brady F, Pike VW, *et al.* Preparation of human serum [methyl-^{11}C] methylalbumin microspheres and human serum [methyl-^{11}C] methylalbumin for clinical use. *Int J Appl Radiat Isotop* 1984; 35: 337–344.
23. West JB, Holland RAB, Dollery CT, Mathews CME. Interpretation of radioactive gas clearance rates in the lung. *J Appl Physiol* 1962; 17: 14–20.
24. Brudin LH, Rhodes CG, Valind SO, Jones T, Jonson B, Hughes JMB. Relationships between regional ventilation and vascular and extravascular volume in supine humans. *J Appl Physiol* 1994; 76: 1195–1204.
25. Salazar E, Knowles JH. An analysis of pressure-volume characteristics of the lungs. *J Appl Physiol* 1964; 19: 97–104.
26. Milic-Emili J, Henderson JAM, Dolovich MB, Trop D, Kaneko K. Regional distribution of inspired gas in the lung. *J Appl Physiol* 1966; 21: 749–759.
27. Glazier JB, Hughes JMB, Maloney JE, West JB. Vertical gradient of alveolar size in lungs of dogs frozen intact. *J Appl Physiol* 1967; 23: 694–705.
28. Wagner PD, Dantzker DR, Dueck R, Clausen JL, West JB. Ventilation-perfusion inequality in chronic obstructive pulmonary disease. *J Clin Invest* 1977; 59: 203–216.
29. Wollmer P, Rhodes CG, Hughes JMB. Regional extravascular density and fractional blood volume of the lung in interstitial disease. *Thorax* 1984; 39: 286–293.
30. Pantin CF, Valind SO, Sweatman M, *et al.* Measures of the inflammatory response in cryptogenic fibrosing alveolitis. *Am Rev Respir Dis* 1988; 138: 1234–1241.
31. Kaplan JD, Trulock EP, Anderson DJ, Schuster DP. Pulmonary vascular permeability in interstitial lung disease: a positron emission tomographic study. *Am Rev Respir Dis* 1992; 145: 1495–1498.
32. Brudin LH, Valind SO, Rhodes CG, *et al.* Fluorine-18 deoxyglucose uptake in sarcoidosis measured with positron emission tomography. *Eur J Nucl Med* 1994; 21: 297–305.
33. Kaplan JD, Calandrino FS, Schuster DP. A positron emission tomographic comparison of pulmonary vascular permeability during the adult respiratory distress syndrome and pneumonia. *Am Rev Respir Dis* 1991; 143: 150–154.
34. Kaplan JD, Calandrino FS, Schuster DP. Effect of smoking on pulmonary vascular permeability: a positron emission tomography study. *Am Rev Respir Dis* 1992; 145: 712–715.
35. Wollmer P, Rhodes CG, Deanfield J, *et al.* Regional extravascular density of the lung in patients with acute pulmonary edema. *J Appl Physiol* 1987; 63: 1890–1895.
36. Wollmer P, Rhodes CG, Allen RM, Maseri A, Fazio F. Regional extravascular lung density and fractional pulmonary blood volume in patients with chronic pulmonary venous hypertension. *Clin Physiol* 1983; 3: 241–256.
37. Gorin AB, Kohler J, DeNardo G. Noninvasive measurement of pulmonary transvascular protein flux in normal man. *J Clin Invest* 1980; 66: 869–877.
38. Gorin AB, Kohler J, DeNardo G. Noninvasive measurement of pulmonary transvascular protein flux in sheep. *J Appl Physiol: Respirat Environ Exercise Physiol* 1978; 45: 225–233.
39. Mintun MA, Dennis R, Welch MJ, Mathias CJ, Schuster DP. Measurements of pulmonary vascular permeability with PET and gallium-68 transferrin. *J Nucl Med* 1987; 28: 1704–1716.
40. Mintun MA, Warfel TE, Schuster DP. Evaluating pulmonary vascular permeability with radiolabelled proteins: an error analysis. *J Appl Physiol* 1990; 68: 1696–1706.
41. Calandrino FS, Anderson DJ, Mintun MA, Schuster DP. Pulmonary vascular permeability during the adult

respiratory distress syndrome: a positron emission tomographic study. *Am Rev Respir Dis* 1988; 138: 421–428.
42. Velazquez M, Kuhn C, Weibel ER, Schuster DP. Positron emission tomographic evaluation of pulmonary vascular permeability: a structure-function correlation. *J Appl Physiol* 1991; 70: 2206–2216.
43. Kaplan JD, Trulock EP, Cooper JD, Schuster DP. Pulmonary vascular permeability after lung transplantation: a positron emission tomographic study. *Am Rev Respir Dis* 1992; 145: 954–957.
44. Dauber IM, Pluss WT, Van Grondelle A, Trow RS, Weil JV. Specificity and sensitivity of noninvasive measurement of pulmonary vascular protein leak. *J Appl Physiol* 1985; 59: 564–574.
45. Rocker GM, Morgan AG, Pearson D, Basran GS, Shale DJ. Pulmonary vascular permeability to transferrin in the pulmonary oedema of renal failure. *Thorax* 1987; 42: 620–623.
46. Bell SD, Myers MJ, Peters AM. Noninvasive techniques for the measurement of extraction fraction and permeability surface area product of ^{99m}Tc-DTPA in the human forearm. *Phys Med Biol* 1993; 37: 1759–1771.
47. Homcy CJ, Stauss HH, Kopiwoda S. Beta receptor occupancy: assessment in the intact animal. *J Clin Invest* 1980; 65: 1111–1118.
48. Hughes B, Marshall DR, Sobel BE, Bergmann SR. Characterization of beta-adrenoceptors *in vivo* with iodine-131 pindolol and gamma-scintigraphy. *J Nucl Med* 1986; 27: 660–667.
49. Delforge J, Syrota A, Lancon J-P, *et al.* Cardiac beta-adrenergic receptor density measured *in vivo* using PET, CGP-12177 and a new graphical method. *J Nucl Med* 1991; 32: 739–748.
50. Staehelin M, Hertel C. [^{3}H]CGP-12177, a beta-adrenergic ligand suitable for measuring cell surface receptors. *J Recept Res* 1983; 3: 35–43.
51. Law MP. Demonstration of the suitability of CGP-12177 for *in vivo* studies of β-adrenoceptors. *Br J Pharmacol* 1993; 109: 1101–1109.
52. Brady F, Luthra SK, Tochon-Danguy H-J, *et al.* Asymmetric synthesis of a precursor for the automated radiosynthesis of *S*-[^{11}C]CGP-12177 as a preferred radioligand for β-receptors. *J Appl Radiat Isot* 1991; 42: 621–628.
53. Jones HA, Rhodes CG, Law MP, *et al.* Rapid analysis for metabolites of ^{11}C-labelled drugs: fate of [^{11}C]-*S*-4-(tert-butylamino-2-hydroxypropoxy)-benzimidazol-2-1 in the dog. *J Chromatog* 1991; 570: 361–370.
54. Luthra SK, Osman S, Steel CT, *et al.* Comparison of *S*-[^{11}C]CGP-12177 metabolism in rat, dog and man using solid phase extraction and HPLC. *J Label Compd Radiopharm* 1993; 32: 504–505.
55. Ueki J, Rhodes CG, Hughes JMB, *et al. In vivo* quantification of pulmonary beta-adrenoceptor density in humans with (S)-[^{11}C]CGP-12177 and PET. *J Appl Physiol* 1993; 75: 559–565.
56. Carstairs JR, Nimmo AJ, Barnes PJ. Autoradiographic visualization of beta-adrenoceptor subtypes in human lung. *Am Rev Respir Dis* 1985; 132: 541–547.
57. Hauck RW, Gengenbach S, Sunder-Plassman L, Fruhmann G, Erdman E. β_2-adrenoceptors in human lung and peripheral mononuclear leukocytes of untreated and terbutaline treated patients. *Chest* 1990; 98: 376–381.
58. Hayes M, Qing F, Rhodes CG, Ind PW, Jones T, Hughes JMB. Human pulmonary beta-receptors are downregulated by two weeks of beta-agonist therapy. *Thorax* 1994; 48: BTS meeting (Abstract), July (Manchester).
59. Qing F, Hayes M, Rhodes CG, Ind PW, Jones T, Hughes JMB. The effects of chronic salbutamol therapy on human β-adrenergic receptors (β-AR): peripheral mononuclear leukocytes (MNL) compared to lung tissue. *Thorax* 1994; 48: BTS meeting (Abstract), July (Manchester).
60. Hwang DR, Eckelman WC, Mathias CJ, Pertrillo EW, Lloyd J, Welch. Positron-labeled angiotensin-converting enzyme (ACE) inhibitor: fluorine-18-fluorocaptopril: probing the ACE activity *in vivo* by positron emission tomography. *J Nucl Med* 1991; 32: 1730–1737.
61. Markham J, McCarthy TJ, Welch MJ, Schuster DP. *In vivo* measurements of pulmonary angiotensin-converting enzyme kinetics. I. Theory and error analysis. *J Appl Physiol* 1995; 78: 1158–1168.
62. Schuster DP, McCarthy TJ, Welch MJ, Holmberg S, Sandiford P, Markham J. *In vivo* measurements of pulmonary angiotension-converting enzyme kinetics. II. Implementation and application. *J Appl Physiol* 1995; 78: 1169–1178.
63. Swenson ER, Rhodes CG, Araujo L, *et al.* Intrathoracic localization and quantitation of tissue carbonic anhydrase in dogs studied with PET. *Physiologist* 1989; 32: 210.
64. Syrota A, Comar D, Paillotin G, *et al.* Muscarinic cholinergic receptor in the human heart evidenced under physiological conditions by positron emission tomography. *Proc Natl Acad Sci* 1985; 82: 584–588.
65. Delforge J, Janier M, Syrota A, *et al.* Noninvasive quantification of muscarinic receptors *in vivo* with positron emission tomography in the dog heart. *Circulation* 1990; 82: 1494–1504.
66. Sokoloff L, Reivich M, Kennedy C, *et al.* The ^{14}C deoxyglucose method for the measurement of local cerebral glucose utilization: theory, procedure, and normal values in the conscious and anesthetized albino rat. *J Neurochem* 1977; 28: 897–916.
67. Patlak CS, Blasberg RG, Fenstermacker JD. Graphical evaluation of blood to brain transfer constants from multiple time uptake data. *J Cereb Blood Flow Metab* 1983; 3: 1–7.
68. Nolop KB, Rhodes CG, Brudin LH, *et al.* Glucose utilization *in vivo* by human pulmonary neoplasms. *Cancer* 1987; 60: 2682–2689.
69. Rege SD, Hoh CK, Glasby JA, *et al.* Imaging of pulmonary mass lesions with whole-body positron emission tomography and fluorodeoxyglucose. *Cancer* 1993; 72: 82–90.
70. Gupta NC, Frank AR, Dewan NA, *et al.* Solitary pulmonary nodules: detection of malignancy with PET with ^{2}-[F-18]-fluoro-2-deoxy-D-glucose. *Radiology* 1992; 184: 441–444.
71. Dewan NA, Gupta NC, Redeppening LS, Phalen JJ, Frick MP. Diagnostic efficacy of PET-FDG imaging in solitary pulmonary nodules. *Chest* 1993; 104: 997–1002.
72. Kubota K, Matsuzawa T, Fujiwara T, *et al.* Differential diagnosis of lung tumor with positron emission tomography: a prospective study. *J Nucl Med* 1990; 31: 1927–1932.
73. Lewis P, Griffin S, Marsden P, *et al.* Whole-body ^{18}F-fluorodeoxyglucose positron emission tomography in preoperative evaluation of lung cancer patients. *Lancet* 1994; 344: 1265–1266.
74. Jones HA, Clark RJ, Rhodes CG, Schofield JB, Krausz T, Haslett C. *In vivo* measurement of neutrophil activity in experimental lung inflammation. *Am J Respir Crit Care Med* 1994; 149: 1635–1639.

75. Matzke K-H, Meyer G-J, Osterholtz A, Coates G, Firnau G. Synthesis of ^{11}C-5-hydroxytryptamine for the measurement of pulmonary endothelial cell function. *Int J Appl Radiat Isot* 1991; 42: 401–404.
76. Coates G, Firneau G, Meyer G-J, Gratz KF. Noninvasive measurement of the lung carbon-11 serotonin extraction in man. *J Nucl Med* 1991; 32: 729–732.
77. Syrota A, Pascal O, Crouzel M, Kellershohn C. Pulmonary extraction of C-11chlorpromazine, measured by residue detection in man. *J Nucl Med* 1981; 22: 145–148.
78. Morel DR, Dargent F, Backmann M, Suter PM, Junod AF. Pulmonary extraction of serotonin and propranolol in patients with adult respiratory distress syndrome. *Am Rev Respir Dis* 1985; 132: 479–484.
79. Wollmer P, Rhodes CG, Pike VW, *et al*. Measurement of pulmonary erythromycin concentration in patients with lobar pneumonia by means of positron emission tomography. *Lancet* 1982; ii: 1361–1364.
80. Syrota A. Receptor binding studies of the living heart. *In*: New Concepts in Cardiac Imaging. Year Book Publishers Inc., 1988; 4: pp. 141–166.